The Vertical Structure of Cloud Occurrence and Radiative Forcing at the SGP ARM Site as Revealed by 8 Years of Continuous Data

GERALD G. MACE AND SALLY BENSON

Department of Meteorology, University of Utah, Salt Lake City, Utah

(Manuscript received 11 April 2007, in final form 24 August 2007)

ABSTRACT

Data collected at the Atmospheric Radiation Measurement (ARM) Program ground sites allow for the description of the atmospheric thermodynamic state, cloud occurrence, and cloud properties. This information allows for the derivation of estimates of the effects of clouds on the radiation budget of the surface and atmosphere. Herein 8 yr of continuous data collected at the ARM Southern Great Plains (SGP) Climate Research Facility (ACRF) are analyzed, and the influence of clouds on the radiative flux divergence of solar and infrared energy on annual, seasonal, and monthly time scales is documented. Given the uncertainties in derived cloud microphysical properties that result in calculated radiant flux errors, it is demonstrated that the ability to quantitatively resolve all but the largest heating and cooling influences by clouds is marginal for averaging periods less than 1 month. Concentrating on seasonal and monthly averages, it is found that the net column-integrated radiative effect of clouds on the atmosphere is nearly neutral at this middle-latitude location. However, a net heating of the upper troposphere by upper-tropospheric clouds and a cooling of the lower troposphere by boundary layer clouds is documented. The balance evolves over the course of an annual cycle as the troposphere deepens in summer and boundary layer clouds become less frequent relative to upper-tropospheric clouds. Although the top-of-atmosphere IR radiative effect is nearly invariant through the annual cycle, the seasonally varying heating profile is determined largely by the convergence of IR flux because solar heating is offset by IR cooling within the column.

1. Introduction

The atmospheric hydrological cycle maintains strong nonlinear controls on the manner in which the climate system maintains energetic balance. While overall energetic balance in the atmosphere is maintained by the net loss of radiant energy to space and the net gain of radiant energy from the surface and from latent heat released by precipitation, the manner in which energetic balance is achieved through vertical and horizontal transports within the atmospheric circulation largely determines the sensible climate that is experienced at the earth's surface. Because the atmospheric hydrological cycle responds to the circulation while the atmospheric motions are accelerated through production of thermal gradients induced by net diabatic heating, the coupling between the hydrologic cycle and the atmospheric motions represents one of the most fundamental feedback processes within the climate system (Bony et al. 2006; Stephens 2005). Indeed, accurate representation of cloud and precipitation feedbacks in numerical models of the general circulation (GCMs) represents one of the major obstacles to accurately predicting anthropogenically induced climate change (Soden and Held 2006; Cess et al. 1997).

Our understanding of the atmospheric hydrological cycle feedback remains poor for a number of reasons (Stephens 2005), but a significant issue is the time and space scales over which the coupling between the hydrological cycle and the atmospheric circulation occurs. While Rossow and Cairns (1995) show that cloud systems are largely organized and maintained on the synoptic scale, Weaver et al. (2005) show that the cloud and precipitation properties within a midlatitude cyclone respond to very fine temporal- and spatial-scale vertical motions. The tropical atmosphere also shows substantial sensitivity to finescale cloud and precipita-

Corresponding author address: Gerald G. Mace, Department of Meteorology, University of Utah, 201 S 1460 E, Room 819 (819 WBB), Salt Lake City, UT 84112-0110.
E-mail: mace@met.utah.edu

DOI: 10.1175/2007JCLI1987.1

tion feedbacks, such as within the Madden–Julian oscillation (Bony and Emmanuel 2005; Stephens 2005). Even though the synoptic-scale atmosphere responds relatively slowly to the heating induced by clouds, the details of the meso- and smaller-scale processes that produce clouds and precipitation ultimately drive the feedback process. These details include the vertical and horizontal distribution of clouds and their overlap, the microphysical and radiative properties of clouds and precipitation, and the processes and vertical location where precipitation is ultimately produced within the system relative to where the bulk of the radiative heating and cooling takes place.

While GCMs are generally able to capture the gross details of the top-of-atmosphere (TOA) radiation balance (Potter and Cess 2004; Gates et al. 1999), the processes internal to the atmosphere through which this balance is achieved varies widely among the models, as shown by several recent intercomparison studies (Gates et al. 1999; Stephens et al. 2002). This internal disparity results in widely varying climate sensitivities when the models are forced by changing atmospheric composition (Ringer et al. 2006; Soden and Held 2006). The actual parameterization of microphysical properties appears to contribute to these differences (Senior and Mitchell 1993), and certain disparities, when compared to observations, appear to be common among the models (Zhang et al. 2005). However, the macroscopic cloud properties, such as overall cloud occurrence, and the seasonal variability of cloud occurrence and cloud properties differ substantially across GCMs (Zhang et al. 2005). These differences, while disconcerting, are not surprising given the dearth of climatological data describing the vertical distribution of clouds within the atmosphere. While satellite cloud climatologies, such as the International Satellite Cloud Climatology Project (ISCCP), are able to provide some observational constraint (Rossow and Zhang 1995), no comprehensive datasets documenting the vertical distribution of cloud occurrence and properties over seasonal and interannual time scales have been available to the modeling community.

Active remote sensing systems such as millimeter radar and lidar provide vertical profiles of cloud occurrence and cloud properties, and datasets that are of potential use for validating GCMs and developing new parameterizations are now being created by both ground- and space-based systems (Mace et al. 2007; Zhang et al. 2007). We have recently described a methodology to merge various active and passive remote sensing data streams collected at the Atmospheric Radiation Measurement (ARM) Program's Climate Research Facility (ACRF; Ackerman and Stokes 2003) near Lamont, Oklahoma, into a single, integrated description of the physical state of the atmospheric profile (Mace et al. 2006b, hereafter Part I). By applying this methodology to 1 yr of data collected at the Southern Great Plains (SGP) ACRF and validating it with surface and TOA radiative measurements, we demonstrated that ground-based data streams are able to represent the atmospheric cloud radiative heating structure with quantitative utility on both seasonal and annual time scales (Mace et al. 2006c, hereafter Part II). In this paper, we extend these earlier studies to consider 8 yr of continuous data collected at the SGP ACRF. Such a long and comprehensive time series from a single location is entirely unique, and allows for exploration of cloud variability and its relationship to the large-scale atmosphere. Evaluation of long-term data also makes the statistics relevant for evaluation of similar quantities derived from general circulation models because the statistics would be representative of regional conditions and not just the specific point at which the data were collected. This long time series also allows us to better quantify the uncertainty of the derived cloud radiative forcing by comparing fluxes at the surface and TOA.

2. Methodology and validation

The primary purpose of the ACRF is to provide continuous measurements that describe the physical state of the atmospheric column above the ground sites so that the representation of clouds and radiation in climate models can be improved (Ackerman and Stokes 2003). Measurements from operational passive and active vertically pointing remote sensors are collected from a suite of ground-based instruments. In addition to the remote sensing measurements, radiosondes are launched on a more or less regular basis to characterize the time-evolving thermodynamic structure of the atmosphere. While these measurements are routinely calibrated and provided to the climate research community, there is considerable inertia in taking the basic data streams collected at the ARM central facilities and converting those data streams into a description of the atmosphere that is useful for understanding the long-term variability in cloud properties and radiative forcing. Described fully in Part I, we have been developing tools that facilitate such a description of the atmospheric column physical state. This description includes the thermodynamics, cloud occurrence, cloud microphysics, cloud radiative properties, and up- and downwelling solar and IR flux profiles on a 5-min temporal and 90-m vertical grid valid at the ground site central facilities where the vertical profiles are collected. For

brevity, we term this set of procedures the column physical characterization (CPC).

a. A description of the column physical characterization technique

We begin with atmospheric thermodynamic profiles that are derived by merging the radiosonde record created at the ACRF central facility (CF) with other information such as model output where soundings are missing. The water vapor profiles are scaled with the microwave radiometer (MWR) vapor paths and corrected for dry bias in the upper troposphere using Miloshevich et al. (2001). These data are interpolated to the temporal and vertical resolution of our working grid.

The presence of clouds is observed with vertically pointing millimeter radar and micropulse lidar (MPL) systems at the ACRF central facility. Cloud properties are derived from the remote sensing data using a suite of cloud property retrieval algorithms and parameterizations. We presently use the algorithm of Dong and Mace (2003) to derive cloud properties of warmer-than-freezing layers and the algorithms described by Mace et al. (1998, 2002) for determining the properties of cirrus clouds. When results from the cirrus algorithms are not available, we use the Liu and Illingworth (2000) scheme.

One of the more complex issues (discussed in detail in Part I) is the existence of clouds between the freezing level and about 243 K that could contain both ice and water. In this region relatively large ice crystals dominate the cloud radar signal. We assume that clouds colder than 243 K are composed entirely of ice. When potentially mixed phase clouds exist above warm boundary layer clouds, it is necessary to estimate what fraction of the column water path observed by the MWR is due to the warm clouds so that the Dong and Mace (2003) algorithm can be applied to the liquid phase warm layer. It is also necessary to estimate the microphysical properties of the ice and liquid components of the supercooled/mixed phase portion. To address these issues, we use a parameterization of the liquid cloud profile by Kiehl et al. (1998) and the millimeter wavelength cloud radar (MMCR) cloud occurrence profile to first estimate the fraction of the liquid water path (LWP) observed by the MWR that is warmer than freezing. The ice phase of mixed phase clouds are estimated using a regression-based parameterization of ice water content (IWC) as a function of Doppler velocity (V_d), radar reflectivity factor (Z_e), and temperature derived from aircraft measurements in deep ice phase and mixed phase clouds over the ACRF during March 2000. The liquid phase properties of mixed phase clouds are then estimated using the cold fraction of the MWR water column and the Kiehl et al. (1998) parameterization from which particle sizes are also determined for the liquid and ice mixed phase components.

The cloud radiative properties are then calculated from parameterizations for liquid (Slingo 1989; Kiehl et al. 1998) and ice (Fu 1996; Fu et al. 1998). Solar and IR radiative flux profiles are calculated using a delta two-stream radiative transfer algorithm (Toon et al. 1989; Kato et al. 2001; Mlawer et al. 1997). The primary restrictions are that the CPC cannot be implemented when either the MWR or MMCR are wet from dew or precipitation or when V_d and Z_e measurements suggest the profile is dominated by precipitation.

b. Validation of the CPC

Validation of the results and characterization of the errors is crucial to using this product to understand cloud property and radiative forcing variability from data collected at a ground site. The cloud property retrieval algorithms are validated in the individual papers that describe them, and in Part I we also compare the calculated cloud optical depths to the independently derived estimates of optical depth (Min and Harrison 1996). We rely here primarily on radiative closure using observations of downwelling solar and IR flux at the surface and estimates of upwelling solar and IR flux derived from Geostationary Operational Environmental Satellite (GOES) measurements (Minnis et al. 2002). We focus on the radiative closure in overcast skies from the 8 yr of data used in this study. Clearly, radiative closure at the TOA and surface does not unambiguously establish the uncertainty of the cloud microphysical properties since compensating errors are possible. However, our objective with this study is to examine, in a broad sense, how clouds and cloud radiative forcing varies over time. It seems reasonable to assume that if the fluxes at the TOA and surface are well constrained and the locations of clouds are known from observations, then the uncertainties in the radiative properties of the clouds and the radiative effects of the clouds are also reasonably constrained. Therefore, establishing bias and scatter in the boundary fluxes allows us to understand how the cloud radiative effect (CRE; defined as the watts-per-squared-meter difference between the all-sky and clear-sky fluxes at the surface and TOA) and cloud radiative forcing (CRF; defined as the vertical convergence of radiant flux or heating rate into a volume, typically expressed in kelvins per day) would be impacted by errors in the cloud property retrievals. Using the approach discussed

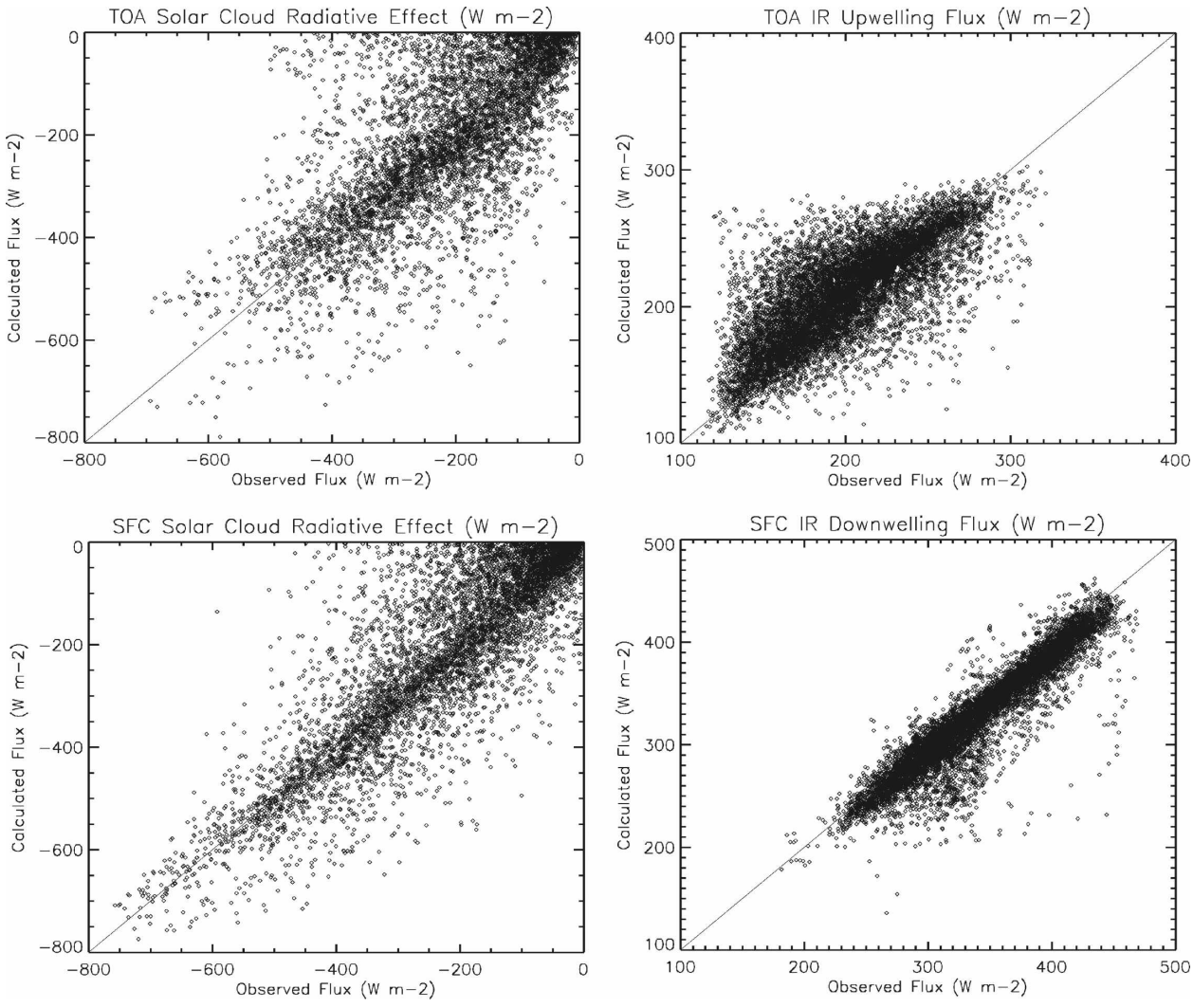

FIG. 1. Comparison of flux calculated using cloud properties derived from the CPC technique to measurements at the TOA and surface (Sfc). Each point in the plots represents a 20-min average from periods of nonprecipitating overcast sky during the period from 1 Jan 1997 through 31 Dec 2004. The statistics of the comparisons are tabulated in Table 1.

in Part II, where standard error propagation techniques were applied using the statistics of the TOA and surface flux comparisons, we derived estimates of error for the up- and downwelling solar and IR fluxes from which we then derived error estimates in the CRE and CRF. The CRF errors are used to bound the heating and cooling estimates of various cloud types during various averaging periods.

Figure 1 shows examples of the comparison of fluxes produced from the CPC and fluxes measured at the ACRF or derived from GOES radiances. Table 1 summarizes the statistics of a more comprehensive set of quantities. Following the notation of Rossow and Zhang (1995), we show the upwelling IR flux ($L_t^{\uparrow}$; W m^{-2}), the upwelling solar flux ($S_t^{\uparrow}$; W m^{-2}), and the solar CRE (CFC − NS; W m^{-2}). At the surface we show the downwelling IR flux ($L_s^{\downarrow}$; W m^{-2}) and the surface solar cloud effect (CFC − NS$_s$). Using clear-sky surface solar flux observations derived from the technique described by Long and Ackerman (2000), we also compare the fraction of the downwelling clear-sky flux that has been removed by cloud (S_Frac$_s^{\downarrow}$) in order to minimize uncertainties associated with aerosols, which we are not attempting to characterize. Overall we find the comparison to observed fluxes encouraging. All quantities show small bias errors of less than 10%, and all quantities have strong linear correspondence to the measurements. In comparison to the solar flux quantities, the scatter about the best-fit lines tends to be smaller for the infrared fluxes. Given the relative im-

TABLE 1. Comparison of CPC-derived radiative flux quantities from overcast nonprecipitating cloud periods with TOA and surface radiation measurements. The averaging time is 20 min for all comparisons. The period included is from 1 Jan 1997 through 31 Dec 2004. All fractional values are reported relative to the mean of the observations. Units of all nonfractional values are W m^{-2}. Following the notation of Rossow and Zhang (1995), $S_t^{\uparrow}$ is the upwelling solar flux (W m^{-2}), $L_t^{\uparrow}$ is the upwelling longwave flux (W m^{-2}), CFC − NS is the solar cloud radiative effect (W m^{-2}), S_Frac$_s^{\downarrow}$ is the fractional change in the downwelling solar flux due to clouds, $L_s^{\downarrow}$ is the downwelling longwave flux (W m^{-2}), and CFC − NS is the net solar cloud radiative effect (W m^{-2}). See the text for additional explanation.

		Median fractional difference	Bias	Correlation coefficient	RMS difference	Slope of linear fit	Intercept of linear fit	Mean obs	Normal deviation	No. of obs
TOA	$S_t^{\uparrow}$	0.13	+0.02	0.81	64	0.91	38	362	93	5665
	$L_t^{\uparrow}$	0.07	+0.05	0.75	19	0.69	70	200.1	24	10 542
	CFC − NS	0.31	+0.03	0.73	105	0.84	−29	−213	103	5548
SFC	S_Frac$_s^{\downarrow}$	0.25	−0.09	0.75	0.21	0.87	0.02	0.529	0.19	6665
	$L_s^{\downarrow}$	0.02	−0.04	0.94	14	0.95	3.7	343	19	10 264
	CFC − NS	0.26	+0.03	0.87	85	0.97	0.43	−213	84	6563

portance of cloud field anisotropy and scattering to solar fluxes coupled with the plane parallel assumption used in the two-stream radiative transfer model, this finding is not surprising. However, the RMS variability tends to be balanced about the 1:1 line, resulting in small bias errors.

Figure 1 and Table 1 are directly comparable to Fig. 13 and Table 5b of Part I. The main difference, of course, between the earlier comparisons and these is the number of individual comparisons in the scatterplots. With a much larger dataset than that used in Part I, our understanding of the error characteristics of the CPC is much improved. While the statistics of the infrared flux comparisons are very similar to those found with a single year's data reported in Part I, we find that the solar flux comparison statistics suggest that our earlier error estimates were optimistic. While the sources for the increased RMS difference can be myriad, examination of Fig. 1 show that, when the solar forcing is small, there is an increased likelihood for the CPC to underestimate the radiative effect of the clouds. We have found that the optical depth distribution of cirrus clouds tends to be exponential, with optically thinner clouds that are much more likely to be observed by the vertically pointing remote sensors than optically thicker clouds (Mace et al. 2001, 2006a). Because the optically thicker cloud elements would tend to dominate the radiative forcing, we would tend to underestimate the solar radiative forcing of cloud fields that tend be thin. Other explanations are possible, of course. It may be that the cirrus cloud property retrieval algorithms bias the optical depth low at some times. Our in situ validation database is too small for a thorough characterization of retrieval uncertainties in the broad cloud-type continuum. This effect is not noticeable in the infrared flux. However, we do find a tendency for a positive bias in $L_t^{\uparrow}$. It is well known that millimeter cloud radars are often unable to sense the tenuous tops of thick cloud systems, and this flux bias is likely a result of that measurement limitation.

The biases in the fluxes at the TOA and surface may imply errors in the time-averaged heating rates to which a large statistical ensemble would converge. With 3% positive biases in both CFC − NS$_s$ and CFC − NS$_t$, we can assume that the solar heating rate bias error would be small, if not negligible. In the infrared, assuming that the clear sky is being modeled correctly, we have a 5% upwelling bias at the TOA and a −4% downwelling bias at the surface. This suggests that the atmospheric CRE and heating rates would be slightly biased toward cooling. This near balance in the TOA and surface biases of the net fluxes is encouraging for statistical analysis of the time-averaged CRE and CRF.

The uncertainty in the CRE and CRF resulting from random, unbiased errors can be estimated from the quantities reported in Table 1 and by using the error covariances in the upwelling and downwelling fluxes (not shown) by applying standard error propagation techniques that are described in Part II. While the uncertainty in the TOA, surface, and atmospheric CRE can be estimated in a straightforward manner from the RMS errors shown in Table 1, deriving the errors in the vertical profile of CRF requires that we assume that the uncertainties in the downwelling fluxes at the surface can be applied to uncertainties in the downwelling fluxes at the lower boundary of each interval in the vertical column, and that the uncertainty in the upwelling fluxes derived from TOA comparisons apply to the upwelling fluxes in each vertical interval. The error covariances between the upwelling and downwelling fluxes are also calculated from simultaneous errors at the surface and TOA. As in Part II, we find a negative

correlation (r) between the TOA and surface flux errors ($r_{solar} = -0.73$, $r_{ir} = -0.15$). This implies that the error covariance has the interesting effect of reducing the impact of flux errors on the heating rate calculations.

Given the substantial uncertainty in deriving cloud properties from remote sensing measurements, these error estimates suggest quantitative bounds on the derived radiative effects and forcings, as illustrated in Table 2, where we present CRE and CRF uncertainties derived from the statistics of the flux comparisons. We find that the uncertainty is often large with respect to the CRE and CRF values that are typically found in the atmosphere (Webster and Stephens 1984; Rossow and Zhang 1995; Part II). For instance, for March 2000 we found that the surface net CRE was on the order of 55 W m^{-2} with an uncertainty of 7 W m^{-2}. On the other hand, the net CRF in the lower troposphere was found to be approximately -1.2 K day^{-1} with an uncertainty of 1 K day^{-1}. Thus, our ability to characterize the CRF quantitatively is limited by our present skill at deriving the cloud radiative properties from the remotely sensed data. We should note, however, that the radiative calculations do not account for cloud field anisotropy, and thus our error estimates are conservative. Regardless, more precise cloud property retrieval algorithms are certainly needed to improve our ability to estimate the CRF with enough precision to resolve the CRF profile quantitatively on finer time scales than is presently possible.

TABLE 2. Uncertainties in the indicated quantities for approximate averaging times.

	1 h	1 day	1 week	1 month
TOA solar CRE (W m^{-2})	53	11	4.1	2.0
TOA IR CRE (W m^{-2})	16	3.3	1.2	0.6
Atmospheric solar CRE (W m^{-2})	55	11	4.2	2.1
Atmospheric IR CRE (W m^{-2})	21	4.5	1.6	0.8
Surface solar CRE (W m^{-2})	15	2.8	1.0	0.5
Surface IR CRE (W m^{-2})	14	2.9	1.1	0.6
Solar CRF (K day^{-1})	16	3.4	1.2	0.6
IR CRF (K day^{-1})	25	5.1	1.9	0.9

3. Results

The ARM data streams are unique in that they simultaneously document the diurnal cycle and the vertical distribution of clouds. These two fundamental aspects of climate system variability are out of reach of most satellite datasets, which are often collected from sun-synchronous orbits and, with the exception of the newly launched *Cloudsat* and *Cloud–Aerosol Lidar and Infrared Pathfinder Satellite Observation* (*CALIPSO*) satellites, can observe only cloud-top or otherwise vertically integrated information from passive radiance and reflectance measurements. Furthermore, while the ARM sites are single points on the earth, measurements over long periods of time do allow for statistical representation of climate states accessible to the geographical regions within which the ARM sites exist (Peixoto and Oort 1992). Assuming that the ARM data from a particular site is representative of at least the regional climate, long-term studies with ARM data can provide valuable insight into the workings of the regional atmosphere that satellite measurements are not able to provide. These insights from observations can provide baselines against which output from global models can be evaluated.

The dataset that we examine here consists of 8 yr of combined active and passive remote sensing measurements and quantities derived from these measurements. A thorough evaluation of this dataset is well beyond the scope of a single paper. In this initial study we consider several aspects of the annual distribution of cloudiness and the radiative effects of clouds, beginning first with the vertical occurrence frequency of clouds and the derived profile of radiative forcing as a function of cloud type. Aspects of the seasonally averaged radiative forcing of clouds, including interseasonal variability, are then considered.

a. Vertical occurrence frequency, CRF, and CRE

Using measurements collected by the MMCR and MPL from January 1997 through December 2004, we find that clouds at some level in the vertical profile occur 48% of the time at the SGP ACRF with a monthly standard deviation of 13% (Table 3). The vertical distribution of cloud occurrence as observed by the active remote sensors (Fig. 2) shows that maxima in cloud occurrence are found 1 and 9 km above the surface, with a well-defined minimum at 3 km. While, clearly, clouds must actually occur before they influence the radiative heating of the atmosphere, many other factors also contribute to the cloud radiative forcing. In addition to radiative properties, such as optical depth that is determined by water path and particle size, the cooccurrence of clouds in the vertical column (i.e., cloud overlap; Mace and Benson-Troth 2002; Naud et al. 2008) as well as their placement within the diurnal cycle also contribute to their radiative influence. Derived from the full 8-yr record, in Fig. 3 we show the overall radiative influence of clouds on the vertical distribution of heating within the atmosphere as a function of cloud type (defined in Table 4), when

TABLE 3. Coverage and monthly coverage standard deviation of cloud coverage observed by the MMCR at the SGP ACRF, expressed in percentages. High, middle, and low clouds are defined as distinct layers that occur above 6.5 km, between 3 and 6 km, and below 3 km, respectively.

	1997–2004		1997–2000		2001–04	
	Coverage	Std dev	Coverage	Std dev	Coverage	Std dev
All clouds	48	13	49	14	48	12
High clouds	34	9	33	11	34	8
Middle clouds	20	9	21	9	20	8
Low clouds	23	13	24	13	21	12

the specific cloud type occurs as an overcast layer during a 1-h period. In Table 5 the radiative effects (CRE) are shown for the TOA, atmosphere, and surface. For these and all other figures, CRE and CRF are shown as vertical and temporal averages when certain specific conditions occur. For the solar radiation quantities, averages over 24 h are used. With respect to the cloud category that includes all overcast periods regardless of type, the net cloud radiative effects at the surface and TOA are both cooling that arises primarily as residuals between the solar albedo effect and net warming in the infrared. The strong radiative effect of overcast clouds as diagnosed from the TOA at this middle-latitude site is experienced almost entirely at the surface with a nearly negligible net radiative effect by clouds on the atmospheric column. However, as discussed in Part II and shown here, this near-zero net radiative effect masks a vertical structure of lower-tropospheric cooling by boundary layer clouds and middle- and upper-tropospheric heating (Fig. 3).

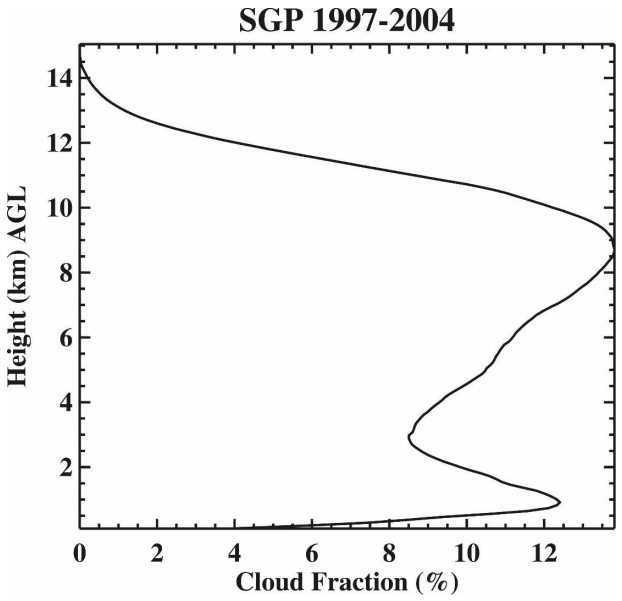

FIG. 2. The vertical distribution of cloud occurrence observed by the MMCR at the SGP ACRF from 1997 to 2004 in 90-m range bins.

Given the large dataset considered, we examine in more detail the cloud-type-dependent radiative heating that results in the vertical structure evident in Fig. 3. From a simple occurrence perspective, high clouds and boundary layer clouds are predominant, as might be expected from the vertical profile in Fig. 2. While thick, high-level clouds dominate the CRF and CRE, their occurrence is small compared to optically thinner high clouds, which have a much more subtle heating influence. We find that thin, high clouds have an overall cooling influence at the TOA and surface that is primarily the result of weak IR warming and solar cooling. The 5 W m^{-2} atmospheric radiative effect is realized primarily by IR warming in the upper and middle troposphere. Thin, high clouds also tend to weakly warm the upper troposphere and cool the middle troposphere, resulting in zero solar CRE. In contrast, thicker high clouds, although much less frequent, have a more significant radiative signature. The 22 W m^{-2} net cooling by thick, high clouds results from a predominant solar albedo effect that is entirely realized as cooling at the surface. However, the neutral atmospheric CRE masks a redistribution of solar energy by high clouds. While thick, high clouds absorb solar radiation and heat the upper troposphere, much of the energy absorbed in the upper troposphere would have been absorbed by middle- and lower-tropospheric water vapor, resulting in a net cloud-induced cooling below the cloud layers. This high-cloud feedback may be much more predominant in convectively active regions of the tropics where thick anvils cover large areas, the water vapor burden of the troposphere is much higher, and the downwelling solar flux is greater. With weak cooling near the tops of thick, high clouds, the TOA IR positive CRE is split nearly evenly between the atmosphere and the surface. While heating is primarily found within the upper troposphere, heating is also realized through the depth of the atmospheric column because downwelling IR flux that would be absent in the clear sky is absorbed in the

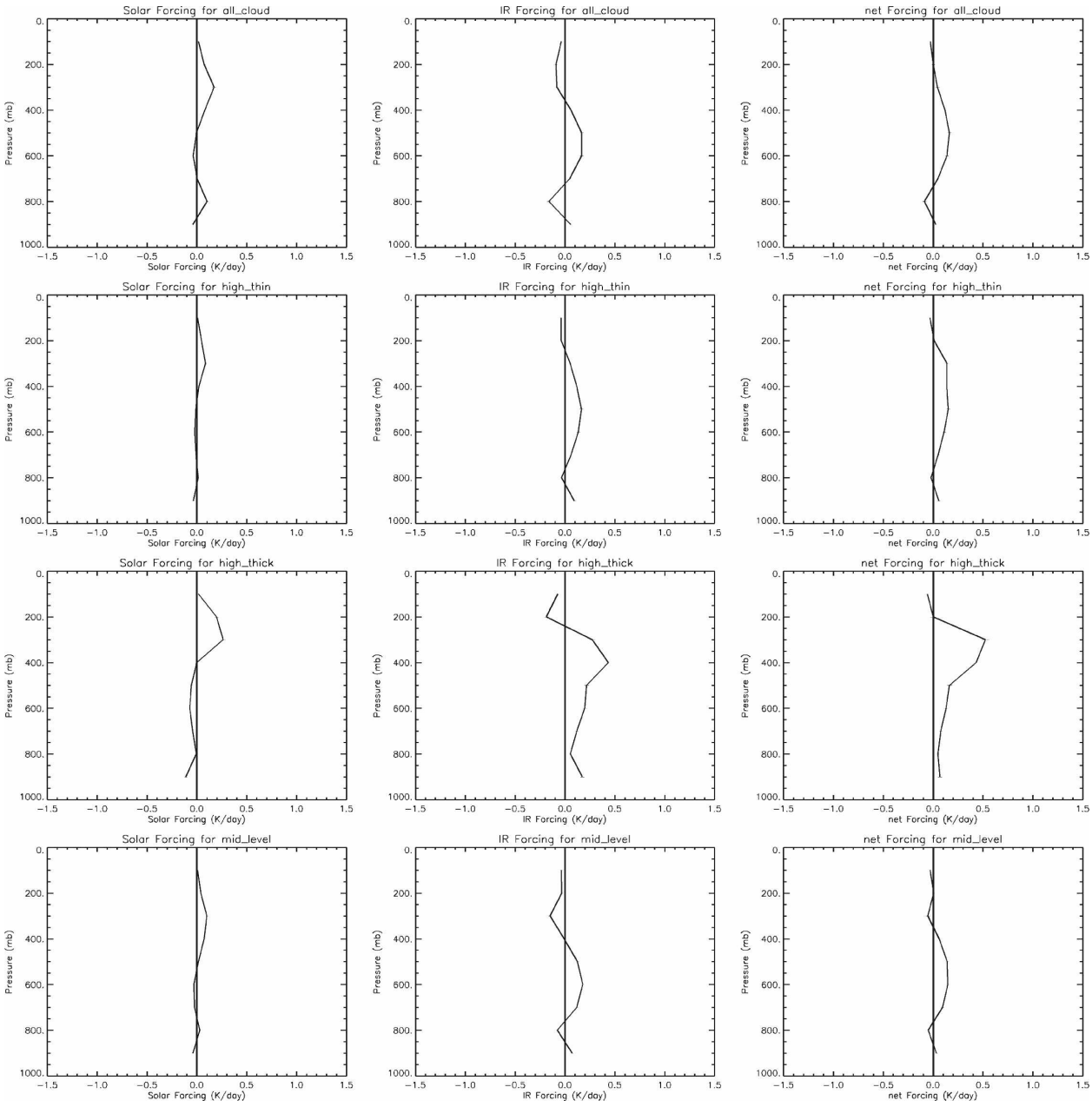

FIG. 3. The vertical distribution of cloud radiative forcing at the SGP ACRF derived using the CPC technique applied to data collected between 1997 and 2004. The data are averaged in 100-mb vertical bins and presented in units of K day^{-1}. Cloud types are defined in Table 4.

subcloud column. The net heating is primarily realized in the upper troposphere where solar heating and IR heating reinforce. In the middle troposphere, the IR heating is predominant while the lower troposphere weakly cools. This result would be highly dependent on when these clouds occur in the diurnal cycle.

Midlevel clouds have less of a net impact than either high- or low-level clouds. Not only do they tend to occur less frequently, but a closer balance seems to exist between heating and cooling in the vertical column, resulting in a smaller net atmospheric CRE. Although the net cooling at the TOA and surface resulting from middle-level clouds is similar to high clouds, the strong couplet between heating at cloud base and cooling near cloud top is more evenly balanced because of the warmer temperatures at which these clouds are found in comparison to cloud layers in the upper troposphere. It is noteworthy also that the relative occurrence of

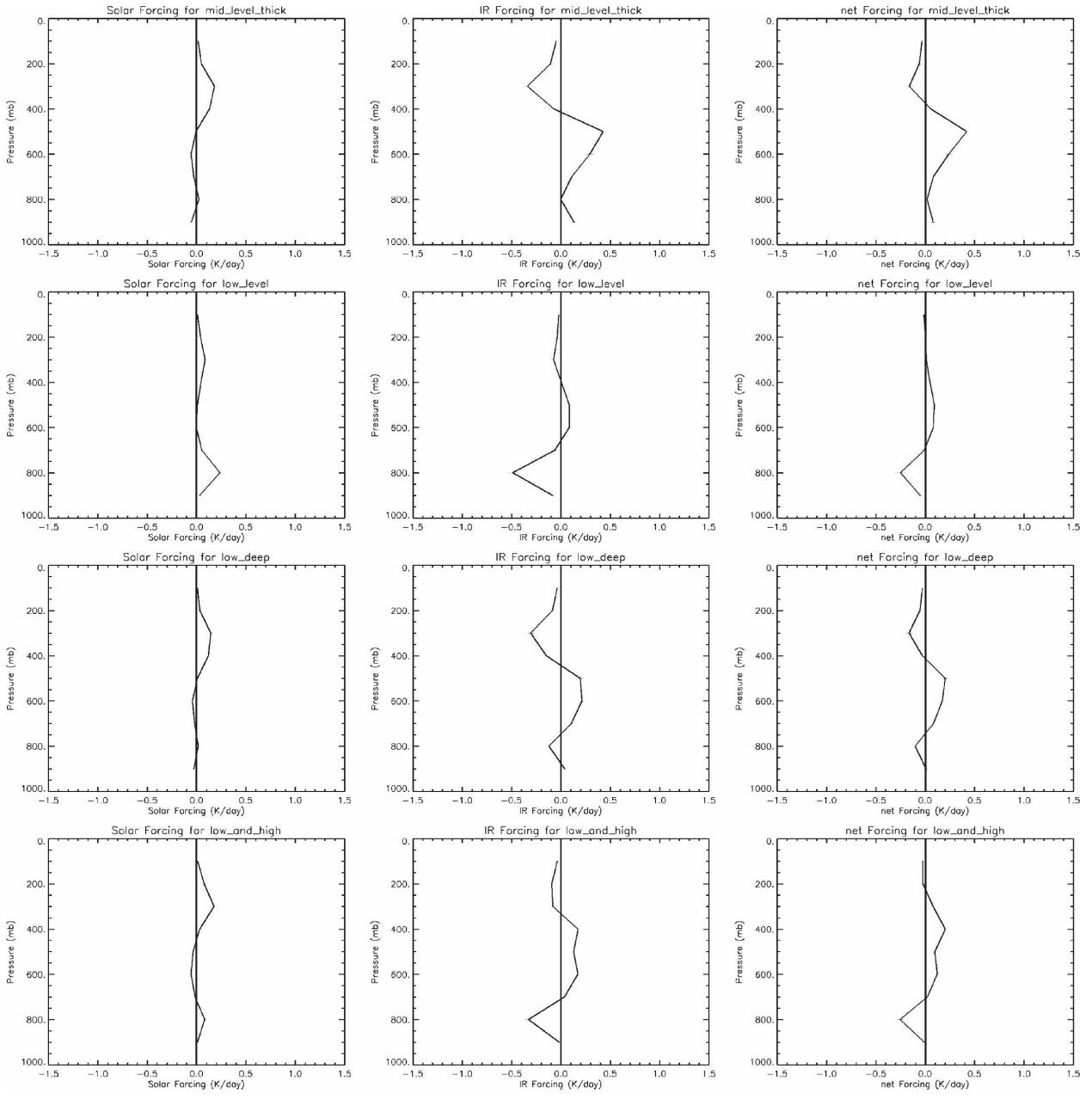

FIG. 3. (*Continued*)

thick and thin midlevel clouds is essentially reversed from what we find in the upper troposphere. This may be, in part, due to the sensitivity of the MMCR, because middle-level liquid water clouds that are not precipitating are known to often have radar reflectivities below the detection threshold of the cloud radar. It is unknown to what degree this biases our statistics, but we think it not significant because in comparisons with MPL data the cloud occurrence in the middle troposphere is only slightly (~5%) greater than that observed from the MMCR alone.

Like other cloud types, low-level clouds have a well-defined cooling influence at the TOA and the surface resulting from a predominance of the albedo effect with a near-neutral overall impact on the atmosphere. However, the strong cooling influence in the lower troposphere, determined primarily by the IR effect of these warm-topped clouds, results in a significant cooling of the lower troposphere. One could argue that because these clouds occur primarily within well-mixed boundary layers, this atmospheric cooling would have been experienced by the atmosphere regardless of the pres-

TABLE 4. Cloud-type definitions. The symbol τ refers to visible optical depth. The "All overcast" classification refers to all overcast periods that include the specific types and also periods that are of mixed type or not classifiable with the other definitions. Adapted from Part I.

Type	Definition
Low clouds	Tops <3 km, $\tau > 0$
Deep, low	Bases <3 km, tops >6.5 km, $\tau > 10$
Thin, middle	Bases >3 km, tops <6.5 km, $\tau < 10$
Thick, middle	3 km < base <6.5 km, top >3 km, $\tau > 10$
Thin, high	Bases >6.5 km, $\tau < 5$
Thick, high	Bases >6.5 km, $\tau > 10$
High–low	Low clouds with high clouds, all τ
All overcast	All bases and tops, all τ

ence of these clouds, yet these clouds are certain to play a strong role in the surface energy balance. For instance, much of the solar energy that is reflected by these clouds would drive convective and evaporative processes at the surface that, in the presence of low-level clouds, would be much less active. Therefore, it is difficult to quantify the true impact of boundary layer clouds from a radiative perspective alone. This subject has been the topic of a great deal of research, especially relating to marine boundary layer clouds. For instance, Bony and Dufresne (2005) identified this issue as a primary climate uncertainty over the subtropical oceans where boundary layer stratocumulus have a well-defined climate impact (Bergman and Hendon 2000; Betts and Ridgway 1989) that global models remain challenged to reproduce. Deep, low clouds have a net CRE similar to that of shallower low-level clouds, yet their influence on the atmospheric heating profile is pronounced. A strong lower-level heating and upper-tropospheric cooling couplet is found with deep, low clouds that is primarily derived from their effects in the infrared. This destabilizing influence on the atmosphere would tend to have a positive feedback on the occurrence of deep, low clouds from a purely radiative perspective.

TABLE 5. The CRE (W m^{-2}) for the full dataset (1997–2004) as a function of the cloud types defined in Table 4. Also included are the number of hours of each cloud type that is included in the average.

		Solar	IR	Net
All cloud (19 441 h)	TOA	−38	+17	−21
	ATM	+2	+1	+3
	SFC	−40	+16	−24
High, thin (4328 h)	TOA	−23	+16	−7
	ATM	+0	+5	+5
	SFC	−23	+11	−12
High, thick (768 h)	TOA	−47	+25	−22
	ATM	+1	+12	+14
	SFC	−48	+13	−35
Midlevel (691 h)	TOA	−29	+25	−22
	ATM	+1	+2	+3
	SFC	−30	+14	−16
Thick, midlevel (1646 h)	TOA	−40	+21	−19
	ATM	+2	+5	+7
	SFC	−42	+17	−26
Low level (3507 h)	TOA	−49	+12	−27
	ATM	+5	−7	−2
	SFC	−54	+19	−35
Low, deep (1277 h)	TOA	−41	+19	−22
	ATM	+1	−1	0
	SFC	−42	+20	−23
Low, high (519 h)	TOA	−43	+18	−25
	ATM	+1	−1	0
	SFC	−44	+19	−25

The overlap of high- and low-level clouds is the most predominant type of layer co-occurrence that can be expected in the atmosphere above the SGP ACRF. Again, this is not surprising given the vertical distribution of cloudiness in Fig. 2. Yet, we find that this overlap of high-over-low clouds tends to be a stabilizing influence on the atmospheric column, even though the net impact of this overlap has a net neutral effect on column-integrated heating.

Overall, this analysis suggests that a delicate balance exists between net cooling in the lower troposphere and heating in the middle and upper troposphere at this midlatitude continental location that is primarily modulated by heating in the thermal IR. This result further suggests that the derived cloud microphysical properties are less important than knowing where, when, and how much cloud of a certain type occurs in the atmosphere. However, while the absorption of solar radiation appears less important from a column-integrated perspective, solar absorption by clouds and the lack of solar absorption by water vapor in the layers beneath a thick cloud layer are important components of the vertical distribution of heating in the troposphere over the SGP ACRF. From this perspective, knowing the microphysical properties of clouds, such as characteristic particle sizes, would be important to understanding how the profile of radiative heating is maintained.

b. Monthly averaged cloud occurrence and CRF

Figure 4 provides the time series of the monthly averaged cloud occurrence statistics over the ACRF from 1997 through 2004. With a 36-s observation interval during most of this period, a 50-mb vertical interval in Fig. 4a contains, on average, 58 000 observations during a 1-month period. We also show the vertical occurrence frequency (hereafter referred to as cloud coverage or cloudiness) in Fig. 4b, defined as the number of times hydrometeor return is observed anywhere within the

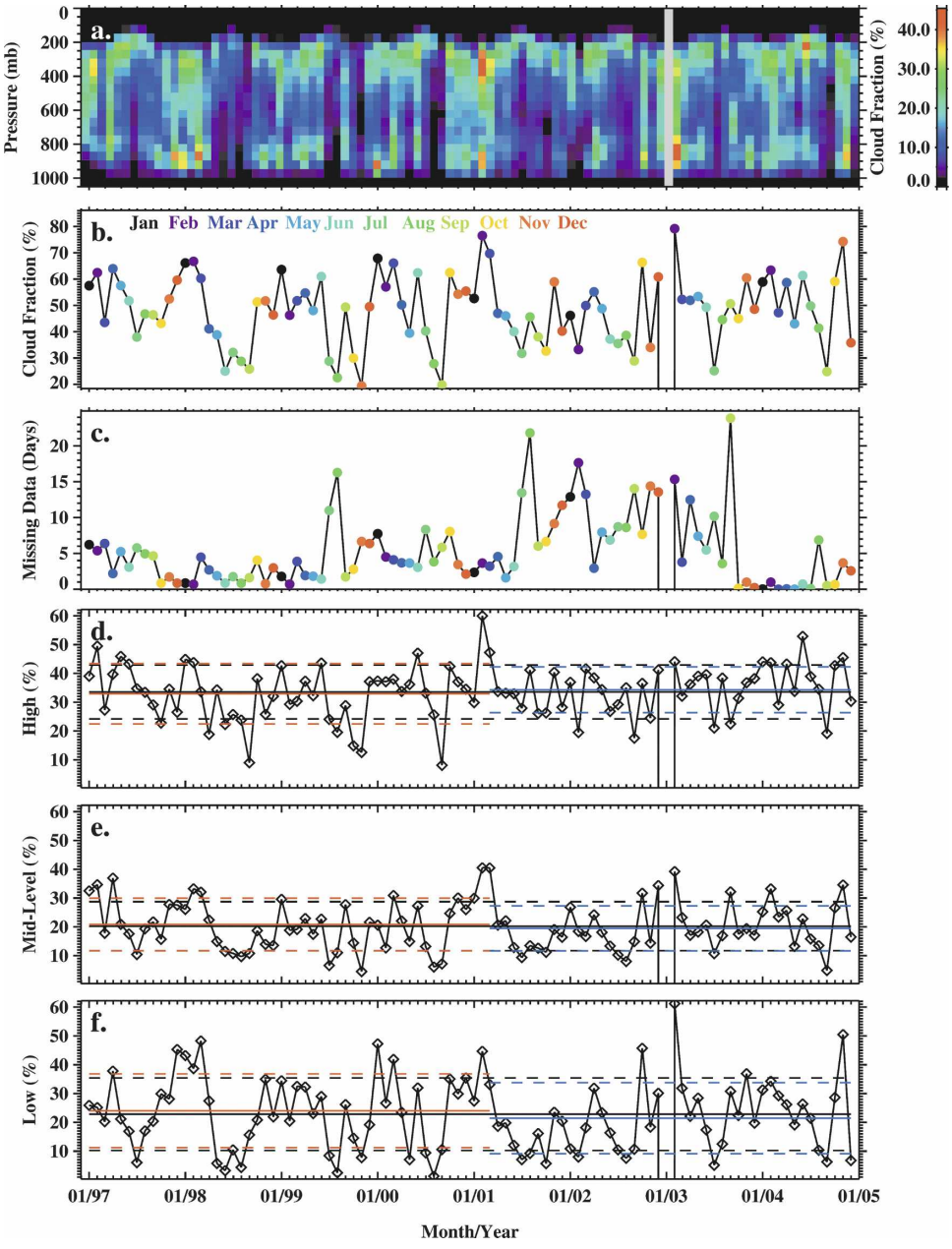

FIG. 4. Monthly averaged cloud occurrence statistics from January 1997 through December 2004 at the SGP ACRF derived from MMCR data: (a) cloud frequency of occurrence in 50-mb vertical range bins, (b) column coverage defined as the number of columns with cloud occurrence in any range bin divided by the total number columns during the month, (c) the number of accumulated days in each month with missing data, and the frequency of the occurrence of (d) high (>6 km), (e) middle (between 3 and 6 km), and (f) low clouds (less than 3 km). In each plot the mean and standard deviation of monthly occurrence is shown by the solid and dashed black lines. The red solid and dashed lines show means and standard deviations for the first half of the record and the blue shows means and standard deviations for the second half of the data record.

vertical profile divided by the total number of profiles observed during an averaging period. While the performance of the MMCR has been excellent over the period under study (Fig. 4c), we do find a slow increase in missing data before October 2003. Only 4 of the 108 months considered have more than half of the days of that month missing. The MMCR was upgraded in October 2003 and the frequency of measurement was im-

proved to 4 s. That change is accounted for in the overall statistics shown here and in later figures.

A clear annual cycle in cloudiness is evident in the time series plots, with the most striking oscillations associated with the seasonal deepening and shoaling of the troposphere. Clouds are typically observed to near 100 mb during midsummer and are rarely observed above 250 mb during winter. While there is substantial month-to-month variability, we find that the mean cloud coverage at the ACRF is 48%, ±13% (Table 3), with maxima reaching nearly 80% in January of 2001 and 2003 and minima as low as 20% in November 1999 and September 2000. Examination of Figs. 4a,b reveals the source of the largest swings in cloudiness over the ACRF, while Figs. 4c,d,f quantify the coverage changes in terms of low, middle, and high clouds. For instance, the period of very low cloudiness during the summer of 1998 was primarily due to a near-total absence of low-level cloudiness. While clouds in the middle troposphere also decreased during this time, high-level clouds did not demonstrate an anomalous minimum during this period. On the other hand, the winter of that year (1997/98) was one of the cloudiest periods in the data record, with clouds at all levels showing anomalously high coverage. We note that this period corresponds to a major El Niño event that was correlated with significant regional anomalies in the southern-central United States (Smith et al. 1999).

Overall, it seems that low clouds (hydrometeor returns from heights less than 3 km) have a slightly higher variability (23% mean coverage, ±13%). Middle-level clouds have a slightly smaller coverage compared to low-level clouds (20%) and demonstrate a smaller monthly variability (9%). High-level clouds occur most frequently (34%, ±9%) with small variability relative to their higher mean occurrence frequency. Finally, while there is some evidence for changes in cloudiness variability during the 8-yr period, neither is there evidence for any type of overall trend in cloudiness nor is there evidence for a trend in cloudiness of specific cloud types defined by vertical location. The length and stability of the cloudiness time series from the MMCR should be considered a resource for validating cloud occurrence datasets derived from satellites, which are, in some circumstances, finding long-term trends in global cloud cover (Cess and Udelhofen 2003) while other analyses suggest that such findings may be erroneous (Evan et al. 2007). It appears from the ground-based measurements at this location that satellite pixels analyzed over the ARM SGP region should show no trend in a long-term analysis of cloud cover.

The annual cycle of the vertically resolved cloud occurrence becomes clearer by examining an annual composite of cloud occurrence and coverage (Fig. 5). The annual cycle of cloudiness at SGP can be broadly separated into a cloudy winter period and the later summer and early fall when cloudiness is at a minimum. The

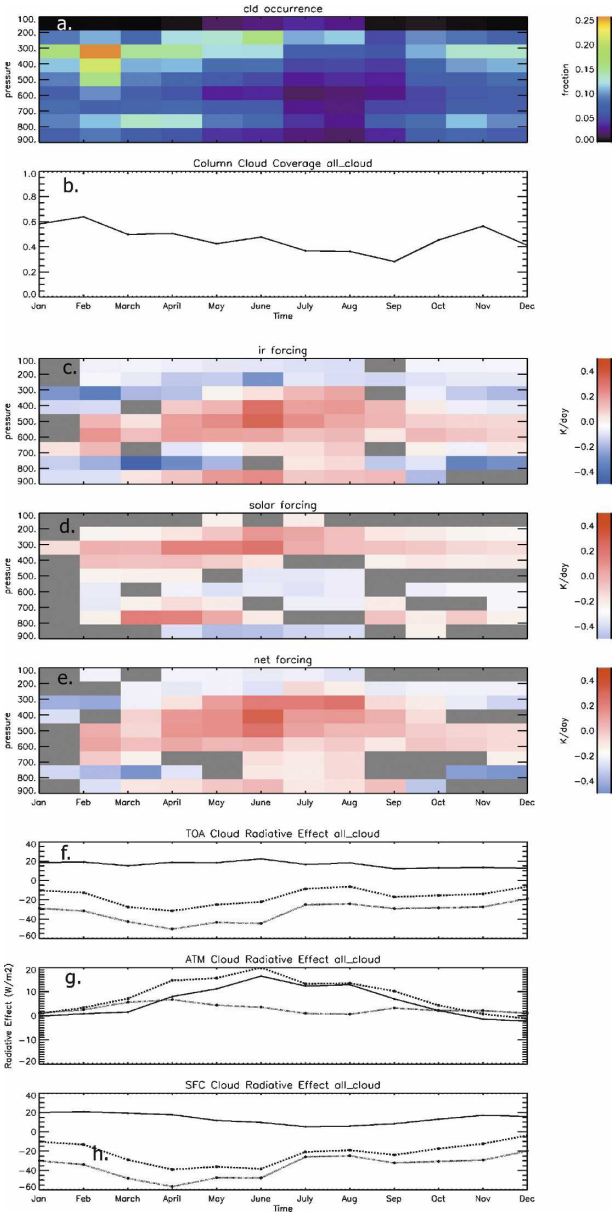

FIG. 5. Cloud occurrence, coverage, radiative forcing, and radiation effects over a composite annual cycle that is derived by averaging all observations collected during a particular month for all years: (a) cloud occurrence in 100-mb vertical bins, (b) cloud coverage, (c) infrared cloud radiative forcing in 100-mb vertical bins, (d) solar cloud radiative forcing, (e) net cloud radiative forcing, and solar (dotted), IR (solid), and net (dashed) cloud radiative effect for (f) TOA, (g) atmosphere, and (h) surface. In (c), (d), and (e), the color gray is used for volumes where the uncertainty in the CRF is more than 20% of the absolute value of the time-averaged CRF in that bin.

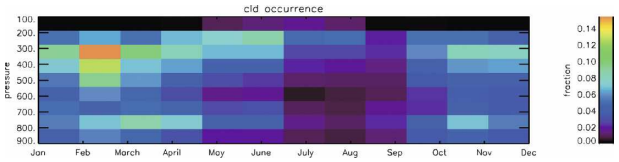

FIG. 6. As in Fig. 5a, but the vertical occurrence is shown under conditions of overcast skies that are used in the analysis of the CRF and CRE.

annual range of monthly averaged cloud cover is approximately a factor 2, with September averaging just 34% coverage compared to February, when cloud cover averages nearly 60%. The predominance of cloudiness in the lower and upper troposphere is evident in Fig. 5a, with distinct minima in cloud occurrence in the middle troposphere during much of the year. The exception to this overall middle-tropospheric minimum occurs during the winter season when synoptic-scale disturbances are more prevalent, although cloudiness in the upper troposphere and boundary layer is still higher overall. While cloudiness throughout the troposphere declines into middle and late summer, the decrease seems to occur at different rates in the vertical column. The middle troposphere begins drying in April while clouds in the lower troposphere begin a steady decline later in the spring. Upper-tropospheric cloudiness persists into midsummer, presumably becoming more associated with convective outflow as the spring advances into summer. The upper-tropospheric clouds do seem to migrate upward during the spring and early summer. The major decline in cloud cover between June and July is primarily due to a decrease in high clouds. We find a fairly sharp increase in cloudiness at all levels in October as synoptic-scale disturbances become more active with a general increase in clouds at all levels as autumn transitions to winter.

The cloud radiative forcing, and the surface, TOA, and atmospheric cloud radiative effects for all overcast cloud periods (Fig. 5) follow the cloud occurrence distributions in a broad sense with very intriguing details evident in the heating and cooling patterns that are related to cloud occurrence and the microphysical properties of the cloud systems. In Fig. 6 we plot the composite cloud occurrence distribution for the subset of overcast periods for which we analyze the cloud radiative forcing and effects. Comparison to Fig. 5a shows that, while the fractional occurrences are smaller by about 10%, the pattern of cloudiness from the entire dataset and the overcast periods is nearly identical, implying that the overall distribution of radiative forcing is reasonably representative of the overall cloud forcing at the SGP site. It is important to remember, also, that the radiative quantities plotted in Fig. 5 and other similar figures are relative to the cloudy periods during the particular averaging period and have not been scaled by the fractional occurrence of overcast clouds. Scaling by cloud occurrences tends to deemphasize the later summer and early autumn heating patterns in Fig. 5.

The net CRF reveals a distinct annual cycle in vertically resolved heating and cooling. The layer responsible for radiative heating of the atmosphere tends to be based near 600 mb throughout the year, with the layer deepening into the summertime upper troposphere where the largest monthly averaged heating is found in cirrus during June. During most of the year, the region centered at 800 mb and the 100-mb depth below the seasonal tropopause is where most of the net atmospheric radiative cooling is concentrated. This cooling is associated primarily with the upper regions of thick ice cloud layers in the upper troposphere and with the tops of boundary layer clouds in the lower troposphere. The radiative cooling is most predominant during the winter season due to thermal IR radiative effects. These effects are largely balanced by absorption of solar radiation in the upper troposphere during the spring and summer and in the boundary layer during early spring.

There are subtle details in the solar and IR heating and cooling balance. Note that during the spring and early summer the solar heating tends to peak in the 300-mb layer, while the majority of the IR cooling takes place above this level closer to the tropopause. This vertical decoupling in heating and cooling would tend to drive thermally forced circulations and has been noted as important to cloud lifetime effects in cloud process models (Starr 1987; Starr and Cox 1985). Because boundary layer clouds are optically thicker near their tops, we do not find this vertical offset in solar and IR heating and cooling in the lower troposphere where infrared radiative cooling has been found to modify the circulation and influence cloud lifetimes and properties (Wang and Albrecht 1986).

The cloud-induced solar cooling in the middle and lower troposphere during late spring and summer is due to reflection of solar radiation by higher clouds. This reflection results in less absorption of solar energy by water vapor than would have occurred in an otherwise clear atmosphere (also discussed in Part II). This solar cooling is largely balanced by absorption of IR radiation emanating from the bases of thick cloud layers. Because of the near balance between solar cooling and IR heating effects in many situations, the occurrence of clouds within the diurnal cycle clearly plays a major factor in the net effects of clouds on atmospheric diabatic processes.

The annual cycle in CRE demonstrates that the overall column cooling by clouds is principally determined by reflection of solar radiation during the spring and early summer and that cooling is realized primarily at the surface (Stephens 2005); note that the atmospheric solar CRE ranges from a maximum of +5 W m^{-2} in April to a minimum near 0 W m^{-2} in August. The infrared CRE at the TOA and surface does not demonstrate large annual swings as does the solar CRE. At the TOA, the IR CRE varies by 4 W m^{-2} from an annual mean of 17 W m^{-2} while the IR CRE at the surface has a range of about 10 W m^{-2} from an annual mean of 16 W m^{-2}. However, the TOA and surface IR CRE annual cycles are different and that difference tends to drive a seasonal cycle in atmospheric IR CRE that is evident in the vertically resolved composite annual cycle. The TOA IR CRE remains nearly constant near 18 W m^{-2} during the first half of the year and then decreases slightly. However, the surface IR CRE begins a steady decline in February with the decline persisting until July when the surface IR CRE begins to increase again. The behavior of the surface IR CRE is predominantly due to the seasonal decline of low-level cloudiness while the TOA IR CRE is much more dependent on the presence of high-level clouds that do not decrease as rapidly or as much as low-level clouds during the spring and summer. The result is an IR heating of the atmosphere as discussed earlier that peaks near 10 W m^{-2} during June. Because the solar CRE plays little role in the atmospheric CRE, the IR variability principally determines the annual cycle of CRE in the atmosphere above this midlatitude continental location.

c. *Seasonal variability of cloud occurrence and CRF*

While the ARM SGP dataset falls far short of what would normally be used for a climatological analysis of variability, it is interesting nonetheless to examine how the eight annual cycles collected by the ARM active remote sensors that we analyze here compare with each other. We consider the individual seasons and the variability associated with cloud occurrence, cloud coverage, and the radiative influence of the clouds on the atmospheric CRF, and the CRE at the TOA and surface (Figs. 7–10). A cursory glance through the figures reveals that the seasons, while substantially different from one another, do not demonstrate a great deal of interannual variability among themselves. Each season has certain distinct characteristics in cloud occurrence and associated radiative influence with anomalies in CRF and CRE that are mostly associated with anomalies in the distribution of cloudiness from one year to another.

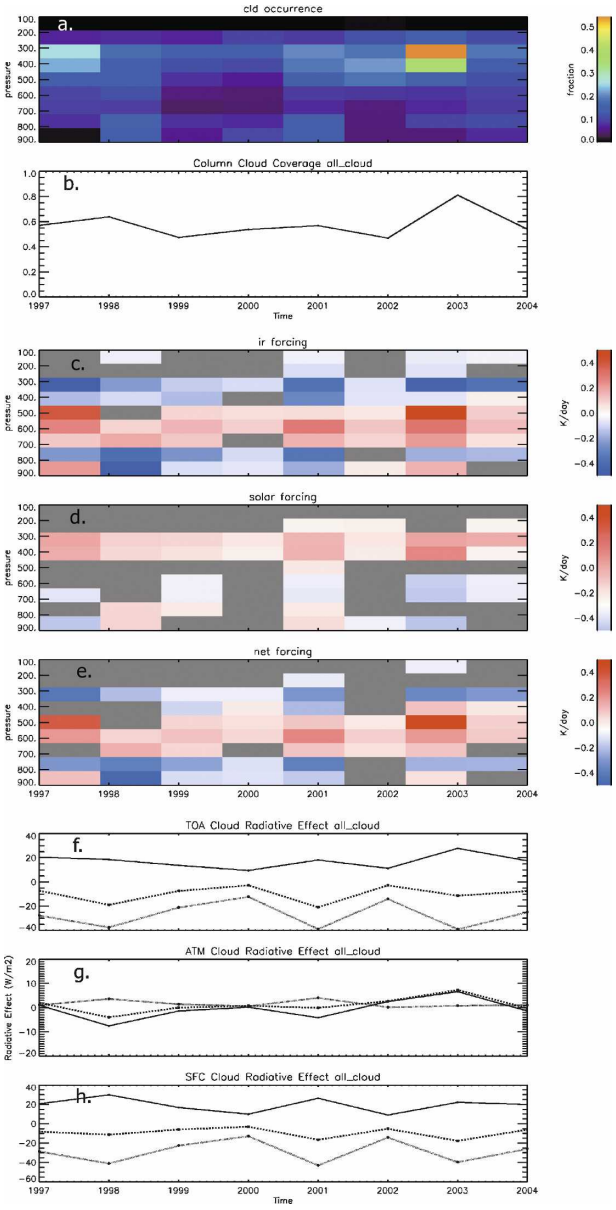

FIG. 7. As in Fig. 5, but the seasonal averages of DJF are shown for each year from 1997 through 2004.

The winter season [December–February (DJF)] in Fig. 7 has the highest cloud cover and also the greatest year-to-year variability in both cloud cover and CRE. Recall that the CRE and CRF refer to the periods only when overcast clouds are present; the actual forcing requires normalizing the radiative quantities by the cloud fraction. Viewing the CRF and CRE in this way allows us to evaluate the effects of cloud location and cloud properties. The winters of 1998 and especially 2003 have the largest cloud cover and the largest TOA CREs. It appears that 1998 and 2001 have a higher-than-normal occurrence of boundary layer

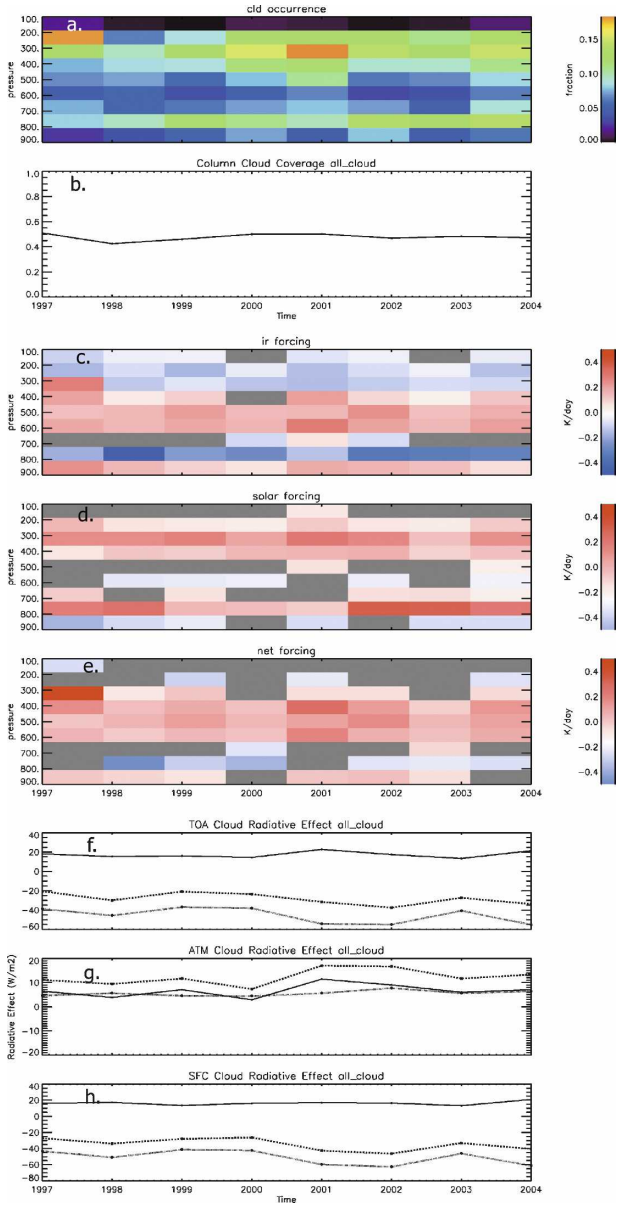

FIG. 8. As in Fig. 7, but March, April, and May are shown.

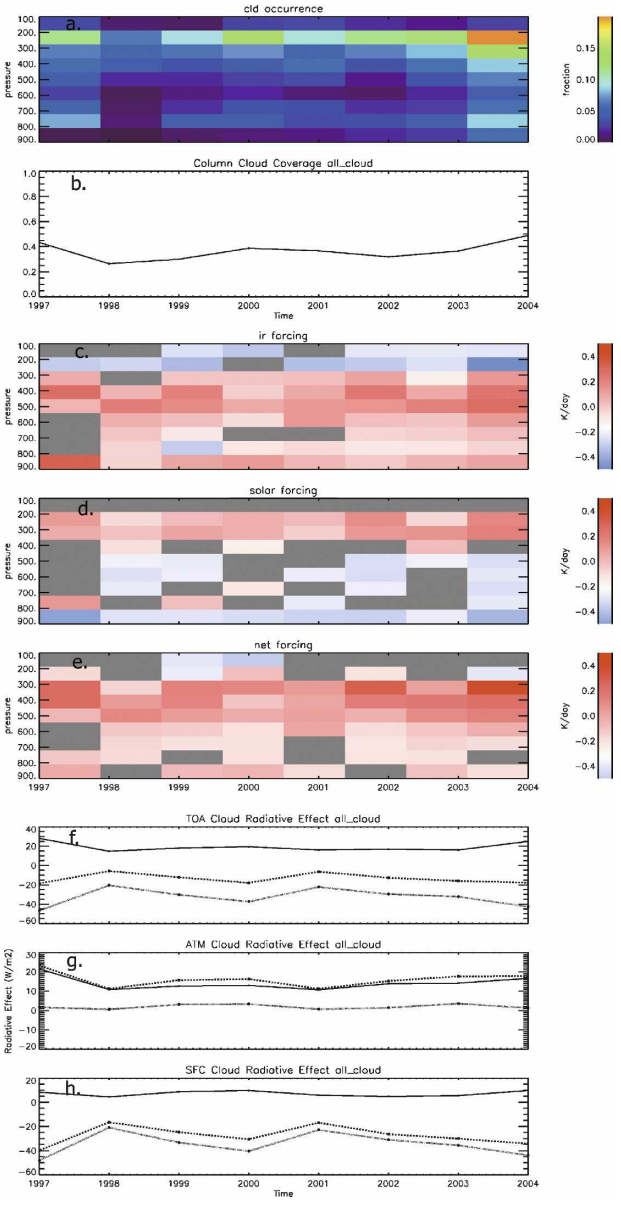

FIG. 9. As in Fig. 7, but JJA are shown.

clouds, while 1997 and 2003 have a much higher-than-average occurrence of cloudiness in the upper troposphere. These changes in distribution influence the CRF in the atmosphere, with 1998 and 2001 showing strong middle-troposphere CRF with offsetting cooling in the upper troposphere and in the boundary layer. With anomalous high clouds in 1997 and 2003, heating associated with the cloud base and downwelling longwave radiation in the middle troposphere is larger than the cooling in the upper troposphere, resulting in about a $+5$ W m^{-2} CRE in the atmosphere. The atmospheric winter season CRE in other years is effectively zero, even for the years of 1998 and 2001 when cloud cover was anomalously high. The imbalance between upper- and lower-tropospheric clouds in 2003 resulted in a positive net atmospheric CRE concentrated in the middle and upper troposphere.

The spring season shows a definite transition from low sun angles and weak solar forcing during winter. Even though the cloud cover decreases slightly, the vertical distribution of clouds remain nearly the same, and the vertical distribution of IR heating and cooling does not change much from winter. Increased solar heating in the upper troposphere and at the top of the boundary

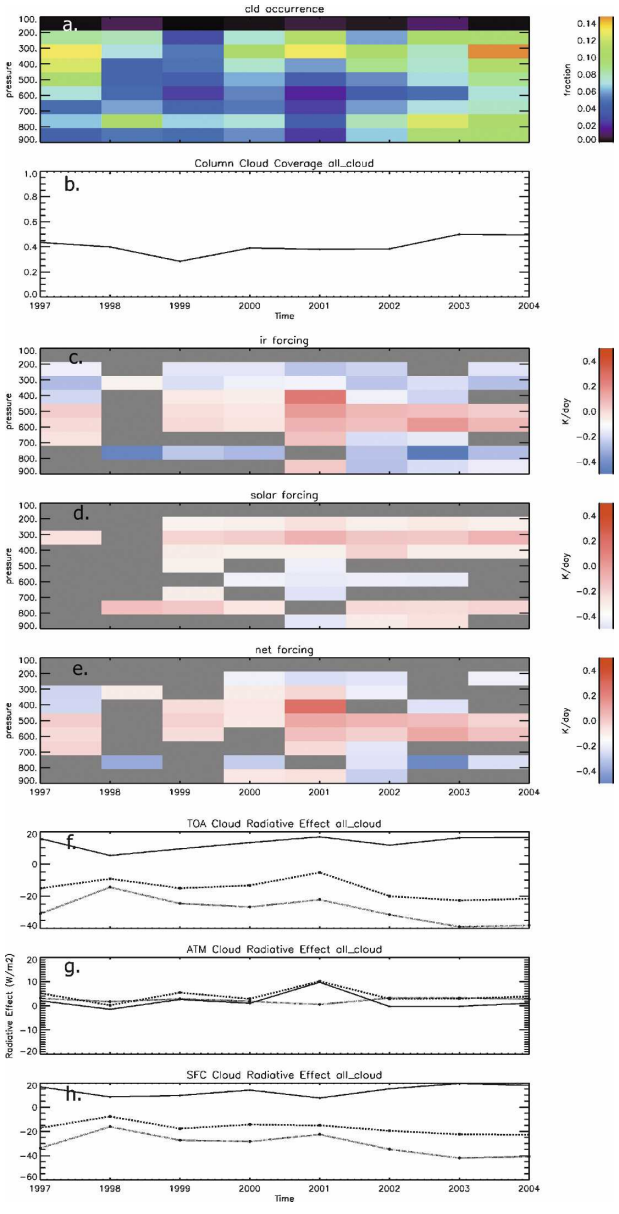

FIG. 10. As in Fig. 7, but SON are shown.

layer largely offsets the IR cooling effects near cloud tops. We find a net positive atmospheric CRE in both the solar and IR that adds to a positive atmospheric CRE that ranges between 10 and 20 W m^{-2}. The interannual variability is small during the eight seasons examined here. Here, 1997, 2000, and 2001 show somewhat higher-than-average upper-tropospheric cloud occurrence resulting in larger-than-average upper-tropospheric heating, especially in 1997 when cirrus were more apt to be found near 200 mb, compared to 2000 and 2001 when cirrus occurrence peaked near 300 mb.

The June–August (JJA) period (Fig. 9) has the lowest average cloud cover of all the seasons, with synoptic-scale weather patterns remaining well north of the Southern Great Plains. The 8-yr period we examine, however, begins and ends in 1997 and 2004 with what appears to be anomalously high cloud cover. In 1997, this high cloud cover appears to be primarily due to higher-than-normal low-level cloudiness, while in 2004 both high and low clouds occur more often than the intervening years when cirrus are the predominant cloud type during the summer season. Examination of the monthly statistics suggests that in the anomalous years, the month of August, which typically has very low cloud cover, is exceptionally more cloudy than normal. The atmospheric CRF is predominantly heating, with the years of anomalous high-cloud occurrence showing increased upper-tropospheric heating compared to other years suggesting that the clouds, when present, had different vertical occurrence distributions and perhaps different microphysical properties compared to other years. The net atmospheric CRE is predominantly due to the IR heating in cirrus since the solar heating is very nearly zero in all years, although the solar CRE at the surface and TOA show year-to-year changes that depend on the properties of high clouds.

The autumn months [September–November (SON)] shown in Fig. 10 mark a transition to more active weather patterns. As discussed above, the month of September is the least cloudy of all months, while November tends to be one of the cloudiest; thus, this period is really one of seasonal transition. Nevertheless, we do find significant year-to-year variability in the vertical distribution of clouds as well as their radiative impacts. With the exception of 1999, when cloud cover was anomalously low, we find little year-to-year variability in cloud cover. It is interesting to compare the years of 1999 with 2001: 1999 had lower-than-average cloud cover, and this decrease in coverage appears to be primarily due to less-than-normal cloudiness in the upper troposphere; 2001, on the other hand, passed with very little low-level cloudiness and much-more-than-normal upper-tropospheric cloudiness. The CRF for these 2 yr are quite different. In 1999, we find weak net heating in the middle troposphere with the CRF in the lower and upper troposphere not resolved above the uncertainty in the calculations. The net CRE in 1999 was weakly positive. In 2001, the lack of clouds in the lower troposphere and thicker-than-normal high-level clouds resulted in strong upper- and middle-tropospheric net heating that is resolved as an anomalously large net CRE primarily due to the IR CRE. Other years demonstrate weak middle-tropospheric net

CRF with solar and IR cooling and heating canceling one another near the tropopause and in the boundary layer.

4. Summary, conclusions, and future work

In this study, we use data collected over an 8-yr period at the ACRF SGP site to examine the statistics of cloud occurrence and the influence of clouds on the radiation budget of the surface, the vertical atmospheric column, and the TOA by examining statistics compiled from the entire dataset, from a composite annual cycle constructed by averaging individual months, and through comparison of seasonal statistics. The approach we take to processing the ARM data into a product that represents a geophysical description of the atmospheric column as a function of time is fully described in Part I and Part II. In this procedure, we begin with the individual calibrated instrument files and then we derive, on a 5-min temporal and 90-m vertical grid, a continuous representation of the thermodynamic profiles, identify clouds in the radar and lidar data, and create a unified description of cloud occurrence as a function of height and time. Cloud property retrievals are implemented and radiative properties are calculated. Finally, the solar and IR flux profiles of clear and cloudy radiation are computed. Validation has been provided through comparison with radiometric fluxes measured at the surface and TOA and through comparison with aircraft data and other validated products. Using the 8-yr dataset, we extend the validation in this study beyond what was presented in Part I and Part II when only a single year of data was considered, although the results are only marginally different. While we show that the overall approach has reasonable skill, the uncertainties in the derived microphysical cloud properties ultimately result in errors in the radiative flux profiles (Table 1). These errors, then, propagate into the calculated CRE and CRF (Table 2). The uncertainty in the CRE and CRF essentially preclude scientific analysis of all but monthly or longer averages of these quantities. We anticipate that future improvements in cloud property retrieval algorithms will allow for reduction of these uncertainties.

The dataset considered here is unique in that it documents the variability of cloud occurrence and properties as well as cloud effects in great temporal and vertical detail over several years. That we are able to examine the full diurnal cycle through the full depth of the troposphere with equal fidelity, regardless of day and night, is a particular advantage of the continuous ground-based data collected by ARM. Much of what we document is not necessarily new in that it has been surmised theoretically (e.g., Stephens and Webster 1981) or inferred from satellite data (e.g., Rossow and Zhang 1995) over the years. We are, however, able to construct a reasonably complete, rigorous, and coherent picture of cloud occurrence, vertical structure, and associated radiative forcing at a particular location that can now be used quantitatively for model validation on monthly and seasonal time scales if the models are sampled appropriately over the region in which the ACRF is located.

Overall, the vertical profile of cloud occurrence is dominated by clouds in the upper troposphere and in the boundary layer at this midlatitude location. Not only do clouds in the middle troposphere occur less often, but the heating and cooling couplets associated with them tend to balance. Upper-tropospheric cloud layers, on the other hand, dominate the heating of the troposphere while lower-level clouds provide a largely counterbalancing cooling influence. The combination of these two cloud types result in little net atmospheric CRE, yet the displacement of the heating and cooling centers in the troposphere would tend to stabilize temperature profiles in a time-averaged sense. Whether or not these patterns of diabatic heating and cooling accelerate or dampen the flows in which they are embedded [i.e., create or destroy available potential energy; see Stuhlman and Smith (1988)] will be the subject of future research. The balance between heating and cooling in the atmosphere is largely due to deposition of thermal infrared flux. While solar absorption cannot be neglected, where it occurs it is largely offset by infrared emission. The exception to this is in the upper troposphere, where solar heating tends to occur at pressures that are higher (lower altitude) than where the majority of the infrared cooling is occurring in thicker clouds. Thus, net solar cooling at the TOA resulting from reflection is largely realized at the surface, and the majority of the net radiative heating in the troposphere is due to IR absorption and emission. This heating and cooling distribution does demonstrate a strong seasonal dependence, with the heating center migrating to lower pressures as the summer troposphere deepens. However, remarkably, this seasonal cycle in IR heating of the troposphere is not evident in the annual cycle of TOA IR CRE and is only weakly evident in the seasonal cycle of the surface IR CRE.

By comparing the time series of seasonal cloud cover and CRE, we find little interannual variability. While there does appear to be some true anomalies in cloud cover (i.e., DJF 2003, JJA 2004), these periods do not result in large anomalies in CRE, suggesting that the distribution and properties of clouds, when they did occur, were not much different from the average. SON

2001 is an example of a significant change in both cloud cover and CRE. During SON 2001, the coverage of upper-tropospheric clouds increased and low-level clouds decreased compared to other years. These changes had a significant influence on the net heating of the atmospheric column and especially on the vertical distribution of that heating. In general, we find that changes in the vertical distribution of clouds on seasonal time scales, while not having a significant influence on the column-integrated CRE, do redistribute diabatic heating within the troposphere, suggesting that a true characterization of the feedback processes of clouds requires a solid understanding of the vertical distribution of that heating, not just a column-integrated measure.

This study is a continuation and natural extension of the methodology and validation papers presented in Part I and Part II. The ARM program was initiated with the principal goal of documenting the occurrence and properties of clouds and detailing the effects that clouds have on the radiation budget of the atmosphere in the geographic regions near the vertically pointing remote sensors (Stokes and Schwartz 1994). The observational objectives of the ARM program are coupled quite naturally with an objective to then use the information gleaned from the data to improve the representation of cloud processes and radiation in climate models. While we would not presume to claim that the observational objectives of the ARM program have been accomplished based solely on our work, the study presented herein does demonstrate that the long-term datasets being created by the ARM program are certainly capable of addressing the climatological variability of cloud occurrence, cloud properties, and the radiative influence of clouds on the surface, TOA, and atmospheric radiation budgets.

There are two principal challenges for future work. First, by comparing appropriately sampled monthly and seasonally averaged model output to these observationally based quantities, we should be better able to document the extent to which climate models are representing atmospheric physical processes and identify where effort should be directed to improve them. A methodology that starts with a comparison of statistics as presented herein and then progresses to case study analyses and eventually process modeling could be a fruitful approach. It would seem in any case, given the existence of long-term statistical datasets like that presented here, that the GCM community must consider how to extract output from their models so that they can be compared rigorously to long-term ground site observations because the ground site observations are beginning to have climatological relevance. The efforts of the Climate Change Prediction Program (CCPP) ARM Parameterization Test bed (CAPT; Phillips et al. 2004) are one example of such an effort. The second immediate challenge is to the observational community. The skill with which we can derive cloud properties from remotely sensed data is not yet sufficient to resolve the diabatic heating structure of particular days, much less individual events. This level of uncertainty is unacceptable and suggests that we are also not yet able to provide rigorous validation of process models. Developing and implementing improved algorithms for cloud property retrievals from remote sensing measurements is clearly needed for continued progress.

Acknowledgments. Funding for this work was supplied by the Environmental Science Division of the U.S. Department of Energy (Grant DE-FG0398ER62571). Data were obtained from the Atmospheric Radiation Measurements Program sponsored by the U.S. Department of Energy Office of Science, Office of Biological and Environmental Research, Environmental Science Division.

REFERENCES

Ackerman, T. P., and G. M. Stokes, 2003: The Atmospheric Radiation Measurement Program. *Phys. Today,* **56,** 38–45.

Bergman, J. W., and H. H. Hendon, 2000: Cloud radiative forcing of the low-latitude tropospheric circulation: Linear calculations. *J. Atmos. Sci.,* **57,** 2225–2245.

Betts, A. K., and W. Ridgway, 1989: Climatic equilibrium of the atmospheric convective boundary layer over a tropical ocean. *J. Atmos. Sci.,* **46,** 2621–2641.

Bony, S., and J.-L. Dufresne, 2005: Marine boundary layer clouds at the heart of tropical cloud feedback uncertainties in climate models. *Geophys. Res. Lett.,* **32,** L20806, doi:10.1029/2005GL023851.

——, and K. A. Emanuel, 2005: On the role of moist processes in tropical intraseasonal variability: Cloud–radiation and moisture–convection feedbacks. *J. Atmos. Sci.,* **62,** 2770–2789.

——, and Coauthors, 2006: How well do we understand and evaluate climate change feedback processes? *J. Climate,* **19,** 3445–3482.

Cess, R. D., and P. M. Udelhofen, 2003: Climate change during 1985–1999: Cloud interactions determined from satellite measurements. *Geophys. Res. Lett.,* **30,** 1019, doi:10.1029/2002GL016128.

——, and Coauthors, 1997: Comparison of the seasonal change in cloud-radiative forcing from atmospheric general circulation models and satellite observations. *J. Geophys. Res.,* **102,** 16 593–16 603.

Dong, X., and G. G. Mace, 2003: Profiles of low-level stratus cloud microphysics deduced from ground-based measurements. *J. Atmos. Oceanic Technol.,* **20,** 42–53.

Evan, A. T., A. K. Heidinger, and D. J. Vimont, 2007: Arguments against a physical long-term trend in global ISCCP cloud amounts. *Geophys. Res. Lett.,* **34,** L04701, doi:10.1029/2006GL028083.

Fu, Q., 1996: An accurate parameterization of the solar radiative

properties of cirrus clouds for climate models. *J. Climate,* **9,** 2058–2082.

——, P. Yang, and W. B. Sun, 1998: An accurate parameterization of the infrared radiative properties of cirrus clouds for climate models. *J. Climate,* **11,** 2223–2237.

Gates, W. L., and Coauthors, 1999: An overview of the results of the Atmospheric Model Intercomparison Project (AMIP I). *Bull. Amer. Meteor. Soc.,* **80,** 29–55.

Kato, S., G. L. Smith, and H. W. Barker, 2001: Gamma-weighted discrete ordinate two-stream approximation for computation of domain-averaged solar irradiance. *J. Amos. Sci.,* **58,** 3797–3803.

Kiehl, J. T., J. J. Hack, G. B. Bonan, B. A. Boville, D. L. Williamson, and P. J. Rasch, 1998: The National Center for Atmospheric Research Community Climate Model: CCM3. *J. Climate,* **11,** 1131–1149.

Liu, C.-L., and A. J. Illingworth, 2000: Toward more accurate retrievals of ice water content from radar measurements of clouds. *J. Appl. Meteor.,* **39,** 1130–1146.

Long, C. N., and T. P. Ackerman, 2000: Identification of clear skies from broadband pyranometer measurements and calculation of downwelling shortwave cloud effects. *J. Geophys. Res.,* **105,** 15 609–15 626.

Mace, G. G., and S. Benson-Troth, 2002: Cloud-layer overlap characteristics derived from long-term cloud radar data. *J. Climate,* **15,** 2505–2515.

——, T. P. Ackerman, P. Minnis, and D. F. Young, 1998: Cirrus layer microphysical properties derived from surface-based millimeter radar and infrared interferometer data. *J. Geophys. Res.,* **103,** 23 207–23 216.

——, E. E. Clothiaux, and T. P. Ackerman, 2001: The composite characteristics of cirrus clouds: Bulk properties revealed by one year of continuous cloud radar data. *J. Climate,* **14,** 2185–2203.

——, A. J. Heymsfield, and M. R. Poellot, 2002: On retrieving the microphysical properties of cirrus clouds using the moments of the millimeter-wavelength Doppler spectrum. *J. Geophys. Res.,* **107,** 4815, doi:10.1029/2001JD001308.

——, S. Benson, and E. Vernon, 2006a: Cirrus clouds and the large-scale atmospheric state: Relationships revealed by six years of ground-based data. *J. Climate,* **19,** 3257–3278.

——, and Coauthors, 2006b: Cloud radiative forcing at the Atmospheric Radiation Measurement Program Climate Research Facility: 1. Technique, validation, and comparison to satellite-derived diagnostic quantities. *J. Geophys. Res.,* **111,** D11S90, doi:10.1029/2005JD005921.

——, S. Benson, and S. Kato, 2006c: Cloud radiative forcing at the Atmospheric Radiation Measurement Program Climate Research Facility: 2. Vertical redistribution of radiant energy by clouds. *J. Geophys. Res.,* **111,** D11S91, doi:10.1029/2005JD005922.

——, R. Marchand, Q. Zhang, and G. L. Stephens, 2007: Global hydrometeor occurrence as observed by Cloudsat: Initial observations from summer 2006. *Geophys. Res. Lett.,* **34,** L09808, doi:10.1029/2006GL029017.

Miloshevich, L. M., H. Vömel, A. Paukkunen, A. J. Heymsfield, and S. J. Oltmans, 2001: Characterization and correction of relative humidity measurements from Vaisala RS80-A radiosondes at cold temperatures. *J. Atmos. Oceanic Technol.,* **18,** 135–156.

Min, Q., and L. C. Harrison, 1996: Cloud properties derived from surface MFRSR measurements and comparison with GOES results at the ARM SGP site. *Geophys. Res. Lett.,* **23,** 1641–1644.

Minnis, P., L. Nguyen, D. R. Doelling, D. F. Young, W. F. Miller, and D. P. Kratz, 2002: Rapid calibration of operational and research meteorological satellite imagers. Part I: Evaluation of research satellite visible channels as references. *J. Atmos. Oceanic Technol.,* **19,** 1233–1249.

Mlawer, E. J., S. J. Taubman, P. D. Brown, M. J. Iacono, and S. A. Clough, 1997: Radiative transfer for inhomogeneous atmospheres: RRTM, a validated correlated-k model for the longwave. *J. Geophys. Res.,* **102,** 16 663–16 682.

Naud, C. M., A. D. Del Genio, G. G. Mace, S. Benson, and E. E. Clothiaux, 2008: Impact of dynamics and atmospheric state on cloud vertical overlap. *J. Climate,* **21,** 1758–1770.

Ockert-Bell, M. E., and D. L. Hartmann, 1992: The effect of cloud type on earth's energy balance: Results for selected regions. *J. Climate,* **5,** 1157–1171.

Peixoto, J. P., and A. H. Oort, 1992: *Physics of Climate.* American Institute of Physics, 520 pp.

Phillips, T. J., and Coauthors, 2004: Evaluating parameterizations in general circulation models: Climate simulation meets weather prediction. *Bull. Amer. Meteor. Soc.,* **85,** 1903–1915.

Potter, G. L., and R. D. Cess, 2004: Testing the impact of clouds on the radiation budgets of 19 atmospheric general circulation models. *J. Geophys. Res.,* **109,** D02106, doi:10.1029/2003JD004018.

Ringer, M. A., and Coauthors, 2006: Global mean cloud feedbacks in idealized climate change experiments. *Geophys. Res. Lett.,* **33,** L07718, doi:10.1029/2005GL025370.

Rossow, W. B., and B. Cairns, 1995: Monitoring changes of clouds. *Climatic Change,* **31,** 305–347.

——, and T.-C. Zhang, 1995: Calculation of surface and top of atmosphere radiative fluxes from physical quantities based on ISCCP data sets. 2. Validation and first results. *J. Geophys. Res.,* **100,** 1167–1197.

Senior, C. A., and J. F. B. Mitchell, 1993: Carbon dioxide and climate: The impact of cloud parameterization. *J. Climate,* **6,** 393–418.

Slingo, A., 1989: A GCM parameterization for the shortwave radiative properties of water clouds. *J. Atmos. Sci.,* **46,** 1419–1427.

Smith, S. R., D. M. Legler, M. J. Remigio, and J. J. O'Brien, 1999: Comparison of 1997–98 U.S. temperature and precipitation anomalies to historical ENSO warm phases. *J. Climate,* **12,** 3507–3515.

Soden, B. J., and I. M. Held, 2006: An assessment of climate feedbacks in coupled ocean–atmosphere models. *J. Climate,* **19,** 3354–3361.

Starr, D. O'C., 1987: Effects of radiative processes in thin cirrus. *J. Geophys. Res.,* **92,** 3973–3978.

——, and S. K. Cox, 1985: Cirrus clouds. Part II: Numerical experiments on the formation and maintenance of cirrus. *J. Atmos. Sci.,* **42,** 2682–2694.

Stephens, G. L., 2005: Cloud feedbacks in the climate system: A critical review. *J. Atmos. Sci.,* **18,** 237–273.

——, and P. J. Webster, 1981: Clouds and climate: Sensitivity of simple systems. *J. Atmos. Sci.,* **38,** 235–247.

——, and Coauthors, 2002: The CloudSat Mission and the A-Train. *Bull. Amer. Meteor. Soc.,* **83,** 1771–1790.

Stokes, G. M., and S. E. Schwartz, 1994: The Atmospheric Radiation Measurement (ARM) Program: Programmatic background and design of the cloud and radiation test bed. *Bull. Amer. Meteor. Soc.,* **75,** 1201–1221.

Stuhlmann, R., and G. L. Smith, 1988: A study of cloud-generated radiative heating and its generation of available potential energy. Part I: Theoretical background. *J. Atmos. Sci.,* **45,** 3911–3927.

Toon, O. B., C. P. McKay, T. P. Ackerman, and K. Santhanam, 1989: Rapid calculation of radiative heating rates and photodissociation rates in inhomogeneous multiple scattering atmospheres. *J. Geophys. Res.,* **94** (D13), 16 287–16 301.

Wang, S., and B. A. Albrecht, 1986: A stratocumulus model with internal circulation. *J. Atmos. Sci.,* **43,** 2374–2391.

Weaver, C. P., J. R. Norris, N. D. Gordon, and S. A. Klein, 2005: Dynamical controls on sub–global climate model grid-scale cloud variability for Atmospheric Radiation Measurement Program (ARM) case 4. *J. Geophys. Res.,* **110,** D15S05, doi:10.1029/2004JD005022.

Webster, P. J., and G. L. Stephens, 1984: Cloud-radiation interaction and the climate problem. *The Global Climate,* J. T. Houghton, Ed., Cambridge University Press, 63–78.

Zhang, M. H., and Coauthors, 2005: Comparing clouds and their seasonal variations in 10 atmospheric general circulation models with satellite measurements. *J. Geophys. Res.,* **110,** D15S02, doi:10.1029/2004JD005021.

Zhang, Y., S. Kein, G. G. Mace, and J. Boyle, 2007: Cluster analysis of tropical clouds using CloudSat data. *Geophys. Res. Lett.,* **34,** L12813, doi:10.1029/2007GL029336.